TOTAL SYNTHESIS AND MOLECULAR DOCKING STUDY OF PEPTIDE AWVDY AS AN ANTI-INFLAMATION AGENT

Anderson Arnold Aloanis*, Jessika Maya Jovanka Najoan, Vlagia Indira Paat, Stefan Marco Rumengan, and Rymond Jusuf Rumampuk

Chemistry Department, Faculty of Mathematics, Natural Sciences and Earth Sciences, Universitas Negeri Manado, Minahasa, Indonesia

ARTICLE INFO	ABSTRACT
Keywords: *Anti-inflammatory peptides; SPPS; oyster; TNF-α; Interleukin-6* *Article History:* *Received: 2025-06-07* *Accepted: 2025-08-05* *Published: 2025-08-18* *d*oi: © 2025 The Authors. This open-access article is distributed under a (CC-BY-SA License)	Bioactive peptides are widely recognized for their diverse biological activities, many of which contribute significantly to human health and well-being. In this study, we synthesized and investigated the anti-inflammatory potential of a peptide sequence, AWVDY, derived from the oyster (*Crassostrea rivularis*). The synthesis was carried out using solid-phase peptide synthesis (SPPS) with the Fmoc strategy on 2-chlorotrityl chloride (2-CTC) resin, resulting in a high yield of 95.91%. The peptide was characterized through Time-of-Flight Electrospray Ionization Mass Spectrometry (TOF-ESI-MS), which identified a peak at m/z [M+H$^+$] 653.1418, corresponding to the expected molecular formula $C_{32}H_{40}N_6O_9$. Analytical HPLC further confirmed the product, showing a retention time of 22.596 minutes. Molecular docking analysis revealed strong binding affinities between AWVDY and the pro-inflammatory cytokines TNF-α and interleukin-6, with values of −10.372 ± 0.013, −10.424 ± 0.005, and −8.946 ± 0.010 kcal/mol, respectively. These results suggest that AWVDY may serve as a dual-target peptide with the potential to modulate inflammatory responses, highlighting its promise as a candidate for future anti-inflammatory drug development.

INTRODUCTION

Bioactive peptides have garnered significant attention as promising therapeutic agents due to their target specificity, biocompatibility, and functional diversity [1, 2]. These peptides exhibit a range of biological activities that contribute to overall health, including roles in digestive health, immune modulation, anti-inflammatory action, and cell signaling processes [3–9]. A variety of bioactive peptides have been successfully isolated from natural sources, with marine animal proteins emerging as particularly rich reservoirs [10]. Among these,

oyster (*Crassostrea rivularis*) proteins have shown potential as a source of peptides with strong reactive oxygen species (ROS) scavenging capacity—an important mechanism in preventing the onset of inflammation [11].

A previous study on *Crassostrea rivularis* identified five major peptides produced through enzymatic hydrolysis, one of which is AWVDY (Ala-Trp-Val-Asp-Tyr) (**Figure 1**). This particular peptide demonstrated potent antioxidant activity, as evidenced by its ability to scavenge DPPH, hydroxyl, and superoxide radicals, with IC$_{50}$

values of 27.50 ± 4.55 µg/mL, 44.00 ± 6.04 µg/mL, and 18.00 ± 3.08 µg/mL, respectively. The presence of valine (Val) and tyrosine (Tyr)—amino acids known for their antioxidant and anti-inflammatory properties—likely contributes to AWVDY's bioactivity [12–14]. Similar peptides containing these residues have also demonstrated both antioxidant and anti-inflammatory effects, including FDPFPK from *Gryllodes sigillatus*, GPRGPPGPVGP from chicken sternal cartilage, VDVPVKVPYS from Baijiu vinasse, and EDDQMDPMAK from foxtail millet [15–18].
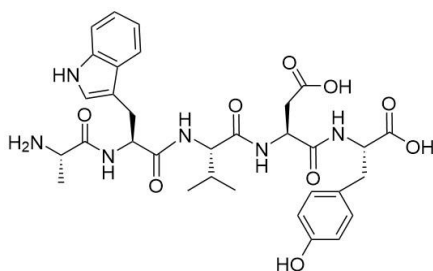

Figure 1. Peptide AWVDY

Due to the limited yield of AWVDY from natural hydrolysates, chemical synthesis is essential to obtain sufficient quantities with high purity and reproducibility—two critical factors for mechanistic studies, formulation development, and potential therapeutic applications. Recent advances in peptide synthesis, particularly the development of efficient synthetic methods and coupling reagents, have significantly improved reaction rates and reduced side reactions [15]. In general, peptide synthesis can be performed using two main approaches: solution-phase synthesis and solid-phase peptide synthesis (SPPS) [16, 17]. Among

these, SPPS is considered more suitable for synthesizing AWVDY due to several advantages, including a simplified purification process. Because the growing peptide chain remains bound to a solid support, it allows for easy separation by filtration and typically yields faster reactions [15].

SPPS has been widely used for the synthesis of therapeutic peptides from marine organisms. For example, it has enabled the production of antihypertensive peptides from *Gracilaria lemaneiformis* and antibacterial peptides from *Streptomyces scopuliridis*, illustrating its pivotal role in facilitating structural, functional, and pharmacological investigations [18, 19]. The Fmoc (9-fluorenylmethoxycarbonyl) strategy is often preferred in SPPS because it allows selective deprotection under mild conditions, minimizing racemization and enabling the production of high-purity peptides [20, 21].

Given its strong antioxidant properties, AWVDY may also possess anti-inflammatory effects, warranting further investigation through computational approaches. Anti-inflammatory peptides (AIPs) are naturally found in various organisms, and many marine-derived peptides—such as LLEL from sturgeon (*Acipenser schrenckii*) cartilage and LGLGAAVL from the marine crab (*Charybdis natator*)—have shown promising anti-inflammatory activity [12, 22]. Inflammation itself is a natural defense mechanism triggered by harmful stimuli such as pathogens, toxins, damaged cells, irritants, or allergens [23].

In this context, *in silico* analysis offers a practical method to explore the anti-

inflammatory potential of peptides like AWVDY. Molecular docking studies commonly target proteins such as interleukin-6 (IL-6) and tumor necrosis factor-alpha (TNF-α), as both play central roles in regulating inflammatory responses [24–26]. IL-6 is a pleiotropic cytokine involved in diverse biological processes, including acute-phase responses, immune cell regulation, blood–brain barrier permeability, synovial inflammation, hematopoiesis, and embryonic development. TNF-α, meanwhile, is a key pro-inflammatory cytokine secreted by immune cells that must be regulated to prevent excessive inflammation [27, 28]. Both cytokines are well-established targets for immunomodulatory therapies, with several successful docking studies supporting their druggability. For example, kirenol has shown strong binding affinity to IL-6, and the peptide KCF18 has demonstrated direct binding to both TNF-α and IL-6 with micromolar-level potency [29, 30].

METHODS

1.   Materials and Tools

Resin 2-Chlorotrityl chloride (CTC)-solid support;   Fmoc-L-Ala-OH, Fmoc-L-Trp(Boc)-OH,   Fmoc-L-Val-OH,   Fmoc-Asp(OtBu)-OH,   Fmoc-L-Tyr(tBu)-OH,   - amino acids;   hexafluorophosphate N-oxide (HATU),   1-Hydroxy-7-azabenzotriazole (HOAt), N, N- Diisopropylethylamine (DIEA) - coupling reagents; N,N-dimethylformamide (DMF) – coupling and washing solvent; dichloromethane (DCM) – capping and washing solvent; methanol (MeOH) – capping reagent; Piperidine, trifluoroacetic acid (TFA), trifluoroethanol (TFE), water (H_2O) – deprotection, cleavage reagent, and chromatography solvent; Diethyl ether – decantation solvent; Acetonitrile (MeCN)-chromatography solvent.

Software tools used in the present study include AutoDock Vina, Auto Dock Tools 1.5.7, Discovery Studio 2025 Client, and Kingdraw. Furthermore, data mining screening was conducted through the PDB website (https://www.rcsb.org/). To obtain the optimized structure of the peptide, the structure was simulated using the PEP-FOLD 4 application developed by Institut Pasteur Biology IT Center and the Ressource Parisienne en Bioinformatique Structurale [31].

The receptor (macromolecule) used in this study is Interleukin-6 (PDB ID:1ALU) and TNF-α (PDB ID:2AZ5). The receptor and reference compound downloaded from the RCSB PDB (Protein Data Bank) in PDB format.

2. Peptide Synthesis

Peptide synthesis manually carried out using the Solid Phase Peptide Synthesis (SPPS) method with the Fmoc strategy on 2-chlorotrityl chloride resin [15].

2.1. Resin Preparation

Weighed 0.400 g of 2-chlorotrityl chloride (CTC) resin and swelled it in 4 mL of dichloromethane (DCM) for 30 minutes at room temperature.

2.2. First Amino Acid Loading

Dissolved 3 equivalents of Fmoc-L-Tyr(tBu)-OH in 3 mL DCM, activated with 1.2 mmol DIEA, and added the solution to the swelled resin. The mixture was gently

agitated for 2 hours at room temperature to facilitate anchoring.

2.3. Capping

After anchoring, unreacted sites on the resin were capped using 5 mL of a MeOH:DCM:DIEA in a 3:16:1 ratio (v/v/v), shaken for 2 × 10 minutes. The step followed by washing the resin with DMF (2mL) and DCM (2×2 mL).

2.4. Resin Loading Quantification

The Fmoc loading was quantified by measuring the UV absorbance of the Fmoc-piperidine adduct at 290 nm using a standard calibration curve.

2.5. Fmoc Deprotection

Deprotection of the Fmoc group was carried out using 4 mL of 20% piperidine in DMF (v/v) for 30 minutes. A chloranil test was then used to verify the presence of free amine groups on the resin, indicated by a color change from blue to red.

2.6. Amino Acid Coupling

Each amino acid was coupled using 3 equivalents of Fmoc-protected amino acid, 3 equivalents of HATU, 3 equivalents of HOAt, and 6 equivalents of DIEA, all dissolved in 4 mL of DMF. The mixture was added to the deprotected resin and agitated for 4 hours at room temperature.

2.7. Post-Coupling Wash and Deprotection

Following each coupling step, the resin was washed with 2 mL DMF and 2 × 2 mL DCM, followed by Fmoc deprotection. Coupling and deprotection steps were repeated for each residue until the full AWVDY sequence was synthesized on the resin.

2.8. Peptide Cleavage and Side-Chain Deprotection

Once peptide assembly was complete, the peptide was cleaved from the resin and the side-chain protecting groups were removed using 3 mL of a cleavage cocktail composed of TFA:water:TIS (95:2.5:2.5, v/v/v). The reaction proceeded for 2 hours at room temperature.

2.9. Peptide Precipitation and Drying

The cleavage solution was dried under vacuum, and 5 mL of cold diethyl ether was added to precipitate the peptide. The mixture was stored at 4°C for 8 hours and then concentrated using a rotary evaporator.

2.10. Characterization

The crude peptide was characterized by Time-of-Flight Mass Spectrometry with Electrospray Ionization (TOF-ESI-MS) to confirm molecular mass. Peptide purity was assessed using analytical HPLC with a Jupiter C18 column (5.0 μm, 4.6 × 250 mm), employing a linear gradient of H_2O:MeCN (10:90 to 90:10) over 60 minutes.

2.11. SPPS Yield

The yield calculation is based on a comparison between the actual amount of purified peptide obtained and the theoretical maximum amount that could be produced, considering the initial resin loading and the molecular weight of the target peptide. The percentage yield is calculated using the following equation 1.

In the equation, the actual peptide weight refers to the dry mass of the purified peptide obtained after cleavage from the resin. The theoretical yield is calculated from the amount of resin used, the loading capacity of the resin (in mmol per gram), and the molecular weight of the target peptide. This calculation provides an estimate of the efficiency of the synthesis process in percentage terms, allowing researchers to evaluate the success and optimization of their SPPS protocols.

$$\text{Yield (\%)} = \frac{\text{Actual weight (g)}}{(\text{Amount of resin (g)} \times \text{Resin loading (mmol/g)} \times \text{MW (g/mmol)})} \times 100\% \quad \text{...............(1)}$$

3. Molecular Docking

Molecular docking simulations were conducted using AutoDock Vina [32] to evaluate the interaction between the AWVDY peptide and pro-inflammatory cytokine receptors. The three-dimensional structures of the receptors and native ligands were prepared using BIOVIA Discovery Studio. After structural optimization, the peptide ligand was converted into the 'pdbqt' format using AutoDock Tools 1.5.7, a process that involved the addition of polar hydrogens and the assignment of torsional flexibility, with all rotatable bonds defined as non-rotatable to simulate peptide rigidity.

The optimized receptor structures, Interleukin-6 (IL-6, PDB ID: 1ALU) and TNF-α (PDB ID: 2AZ5), were prepared similarly and uploaded along with the ligand to define the docking grid box. The grid box was carefully aligned to the binding site of the native co-crystallized ligand in each structure to ensure that the docking process targeted the biologically relevant pocket. Special care was taken to ensure that the entire ligand was fully contained within the grid box boundaries, as this is critical for generating accurate and reproducible docking results.

The generated pdbqt files for both ligand and receptor were placed in the AutoDock Vina working directory. A configuration file was created using a plain text editor (Notepad), specifying key parameters such as receptor and ligand file names, grid box dimensions, and center coordinates. Docking simulations were then executed via the command line interface. The exhaustiveness parameter was set to 100 to ensure a thorough exploration of the conformational space, increasing the chances of identifying the most favorable binding pose [33].

To validate the docking protocol, re-docking of the native ligand into its original binding pocket was performed. The accuracy of the docking was evaluated by comparing the predicted pose with the crystallographic pose using binding free energy values (in kcal/mol) and root-mean-square deviation (RMSD) metrics. An RMSD of less than 2.0 Å was considered indicative of successful docking validation.

To ensure the reliability of results, the docking process for the AWVDY peptide was repeated five times. The results were analyzed based on the calculated binding affinities (ΔG binding), and receptor-ligand interactions were visualized and interpreted using Discovery Studio Visualizer. This included the identification of key amino acid

residues involved in hydrogen bonding, hydrophobic interactions, and electrostatic interactions, displayed through 2D interaction diagrams to facilitate a clear understanding of binding mechanisms.

RESULTS AND DISCUSSION

1. Peptide Synthesis

The synthesis of the AWVDY peptide was performed using the Solid Phase Peptide Synthesis (SPPS) method, which offers efficiency, automation potential, and simplified purification steps. 2-Chlorotrityl chloride (CTC) resin was selected as the solid support due to its mild cleavage conditions, chemical stability during Fmoc deprotection, and its suitability for generating peptides with a free C-terminal carboxylic acid.

The synthesis began with swelling 400 mg of CTC resin in 4 mL of DMF for 30 minutes at room temperature. This swelling process is essential to increase resin surface area and ensure effective interaction with the first amino acid [34]. The first amino acid, Fmoc-L-Tyr(tBu)-OH, was introduced to the swollen resin in 3 mL of DCM, activated with 1.2 mmol of DIEA, and allowed to react for 2 hours under continuous shaking.

After the coupling step, the resin was filtered, washed sequentially with DMF and DCM, and dried. A small sample of the resin was analyzed to determine resin loading—the amount of peptide bound per gram of resin. The calculated resin loading was 0.189 mmol/g. While this is considered relatively low, the synthesis could proceed, as lower loading values can help reduce peptide

aggregation during chain elongation by minimizing steric hindrance and intermolecular interactions [35, 36]. However, this advantage is balanced by a reduced number of peptide chains, which may slightly decrease the final yield.

Before proceeding to the next coupling step, a capping reaction was conducted using a 5 mL mixture of MeOH:DCM:DIEA (3:16:1, v/v/v), shaken twice for 10 minutes. This step is critical to block any unreacted active sites on the resin, preventing undesired chain initiation and minimizing the formation of truncated peptides, thereby improving the final product's purity and simplifying downstream purification [15]. Subsequently, the Fmoc deprotection of the anchored Tyr residue was performed using 4 mL of 20% piperidine in DMF, with shaking for 30 minutes. The resin was then filtered, washed, and dried. To confirm successful deprotection, a chloranil test was conducted by reacting a small amount of the resin with acetaldehyde and p-chloranil solutions. The appearance of a dark red color indicated the presence of free amine groups, confirming that the Fmoc group had been effectively removed.

The second amino acid, Fmoc-Asp(OtBu)-OH, was then coupled using HATU:HOAt:DIEA in a 3:3:6 molar ratio, dissolved in DMF. The reaction proceeded at room temperature for 4 hours. The chloranil test was again used to evaluate coupling success, and the absence of a color change indicated efficient attachment of the second amino acid. This sequential cycle of deprotection and coupling was continued for the remaining amino acids: Fmoc-L-Val-OH,

Fmoc-L-Trp(Boc)-OH, and Fmoc-L-Ala-OH, thus completing the assembly of the AWVDY peptide on the solid support.

The final step involved cleaving the fully assembled peptide from the resin, along with removal of side-chain protecting groups, using a cleavage cocktail composed of TFA:TIS:H_2O (95:2.5:2.5, v/v/v) in a total volume of 3 mL. The reaction was allowed to proceed at room temperature for 2 hours. The filtrate containing the cleaved peptide was collected and concentrated under vacuum. To improve product recovery, the crude peptide was further purified by a decantation procedure using cold diethyl ether, facilitating the removal of residual cleavage reagents and enhancing the yield of the final peptide product.
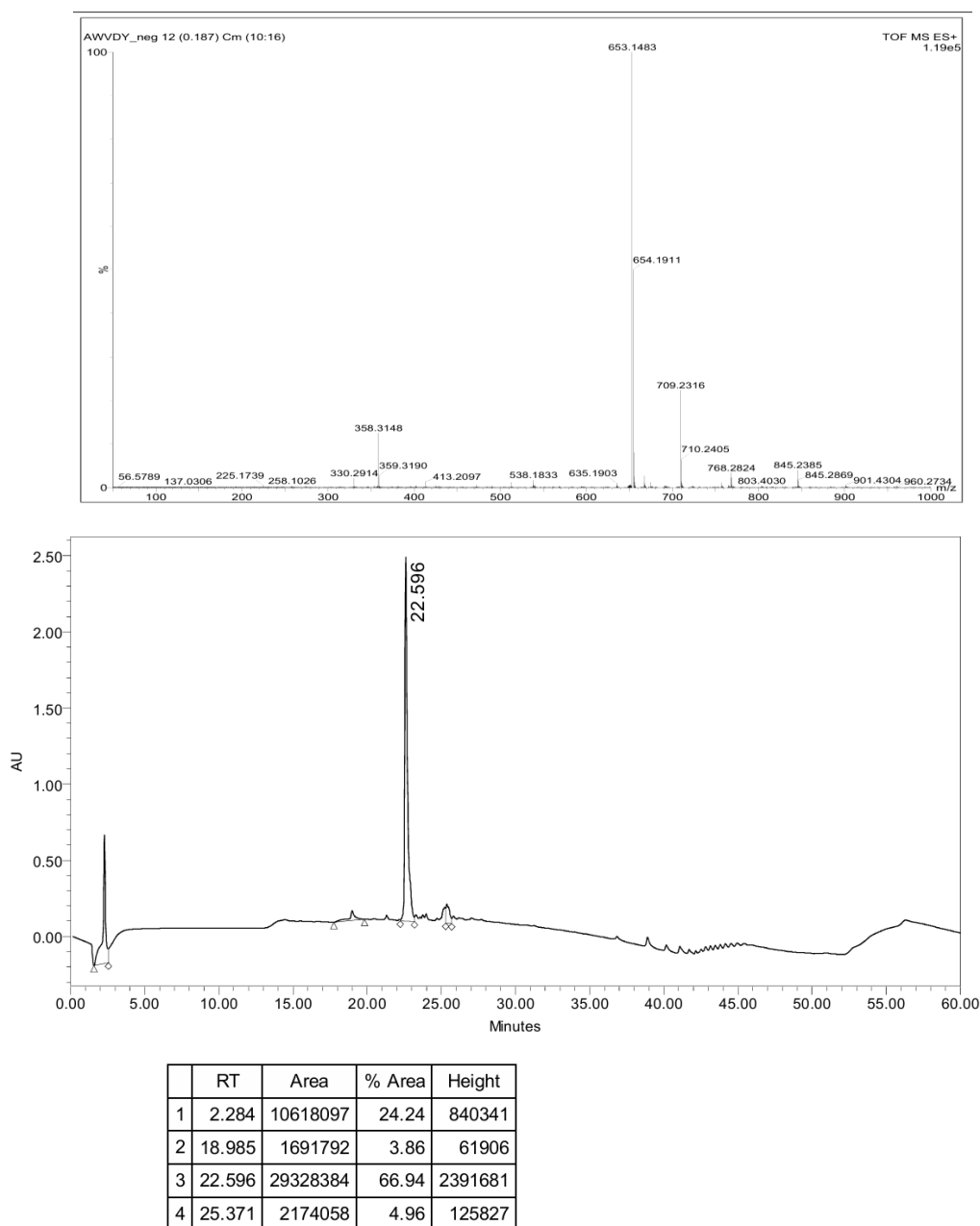

	RT	Area	% Area	Height
1	2.284	10618097	24.24	840341
2	18.985	1691792	3.86	61906
3	22.596	29328384	66.94	2391681
4	25.371	2174058	4.96	125827

Figure 2. ESI-TOF-MS spectrum and analytical HPLC chromatogram of AWVDY

After concentration, the crude peptide was mixed with cold diethyl ether and stored at low temperature (4°C) for 8 hours. Diethyl ether serves as a non-polar solvent that extracts residual impurities—such as scavengers and by-products from the cleavage reaction—while the peptide, being less soluble, precipitates out of solution [37]. The precipitated peptide was then collected by decantation, and the process was repeated twice to improve purity.

Following purification, a total of 47.3 mg of AWVDY peptide was obtained, corresponding to a synthesis yield of 95.91%. The product was characterized using Time-of-Flight Mass Spectrometry (TOF-MS), which revealed a molecular ion peak at m/z [M+H$^+$] 653.1418, consistent with the expected molecular formula $C_{32}H_{40}N_6O_9$. The identity and purity of the peptide were further confirmed via analytical High-Performance Liquid Chromatography (HPLC), showing a retention time of 22.596 minutes (**Figure 2**). The overall synthesis process of the AWVDY peptide is illustrated in **Figure 3**.
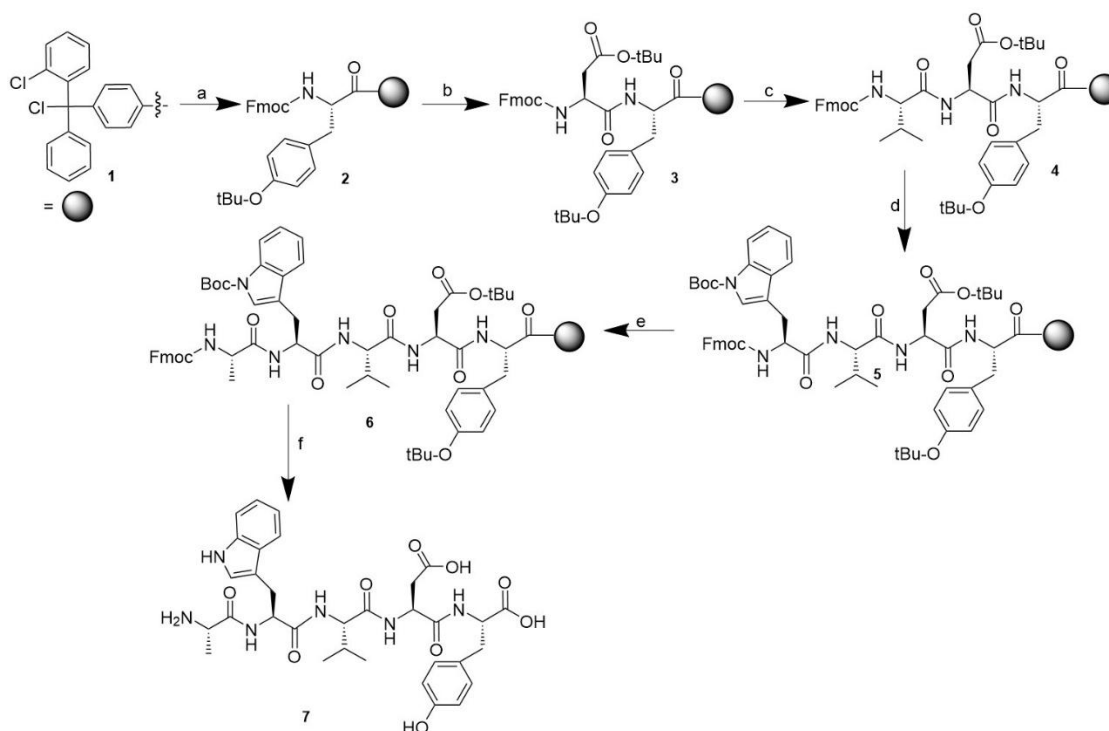

Figure 3. Synthesis of AWVDY. a) a). (1) Fmoc-L-Tyr(tBu)-OH (1 eq), DIEA (2 eq), 4 mL DCM, 4 h, rt; (2) MeOH (15 eq.), DIEA (5 eq.), DCM (80 eq.), 30 min; (3) 20% piperidine in DMF, 30 min. b). (1) Fmoc-L-Asp(OtBu)-OH, (3 eq.), HATU (3 eq.), HOAt (3 eq.), DIEA (6 eq.), 4 mL DMF, 4 h, rt; (2) 20% piperidine in DMF, 30 min. c). (1) Fmoc-L-Val-OH (3 eq.), HATU (3 eq.), HOAt (3 eq.), DIEA (6 eq.), 4 mL DMF, 4 h, rt; (2) 20% piperidine in DMF, 30 min. d). (1) Fmoc-L-Trp(Boc)-OH (3 eq.), HATU (3 eq.), HOAt (3 eq.), DIEA (6 eq.), 4 mL DMF, 4 h, rt; (2) 20% piperidine in DMF, 30 min. e). (1) Fmoc-L-Ala-OH (3 eq.), HATU (3 eq.), HOAt (3 eq.), DIEA (6 eq.), 4 mL DMF, 4 h, rt; (2) 20% piperidine in DMF, 30 min. f). TFA:TIS:H$_2$O (95:2.5:2.5), 3 h, rt.

2.   Molecular Docking

Before docking the test peptide with the target macromolecular receptors, a validation procedure was performed using Interleukin-6 (IL-6, PDB ID: 1ALU) and TNF-α (PDB ID: 2AZ5) to ensure the reliability of

the docking protocol. The validation involved removing the native ligand from the receptor structure using Discovery Studio Visualizer, followed by re-docking the same ligand into its original binding site using AutoDock Vina. The accuracy of the docking setup was assessed based on the root mean square deviation (RMSD) between the predicted pose and the crystallographic pose. A low RMSD value indicates successful reproduction of the native binding conformation, thereby validating the docking protocol.

The docking grid parameters used for AWVDY are presented in **Table 1**. The grid box was designed as a 25 Å cube, specifically chosen to accommodate the flexible, extended conformation of the pentapeptide

AWVDY. Unlike conventional small-molecule ligands, peptides occupy a larger volume and exhibit greater conformational variability. The larger grid size allows for comprehensive sampling of side-chain flexibility, peptide backbone orientation, and potential interactions with secondary or allosteric binding sites—features particularly relevant for dynamic and multimeric proteins like cytokines.

Moreover, this grid dimension ensures that the peptide is not artificially restricted within the docking space, enhancing the biological relevance and predictive accuracy of the docking results, while maintaining acceptable levels of computational efficiency.

Table 1. Grid box coordinate and size

Indicator	Size (1ALU)	Size (2AZ5 site 1)	Size (2AZ5 site 2)
Number of points			
x dimension	25	25	25
y dimension	25	25	25
z dimension	25	25	25
Spacing	0.375	0.375	0.375
Grid center			
x	-7.722	-19.410	-8.334
y	-12.940	74.651	68.217
z	0.048	33.849	19.963

To assess the accuracy and reliability of the docking protocol, a redocking validation was performed using native ligands of both target receptors. For the 1ALU receptor (Interleukin-6), redocking of the native ligand tartaric acid yielded an RMSD of 0.4502 Å, indicating a high level of accuracy in reproducing the ligand's original crystallographic pose (**Figure 4**). This RMSD value, well below the commonly accepted threshold of 2.0 Å, supports the validity and precision of the docking setup.

Similarly, the docking protocol was validated for the 2AZ5 receptor (TNF-α), which features two distinct ligand-binding sites. Redocking at site 1 resulted in an RMSD of 0.3448 Å, while site 2 yielded an RMSD of 0.3463 Å (**Figure 4**). Both values are indicative of accurate binding mode reproduction and further reinforce the robustness of the docking protocol [38].

These consistently low RMSD values demonstrate the method's capacity to replicate experimentally observed binding

conformations with high fidelity. Importantly, achieving such precision in the context of peptide ligands—which are inherently flexible and structurally diverse—suggests that the docking strategy is capable of capturing key molecular interactions and maintaining structural accuracy despite the complexity of the ligand.

Furthermore, these results indicate that the method is not overfitted to rigid small-molecule ligands but instead shows strong generalizability to more complex systems, such as bioactive peptides. This adaptability is critical for meaningful structure-based predictions in peptide-based drug discovery. Overall, the validation provides compelling evidence that the docking protocol is suitable and reliable for investigating the binding behavior of the AWVDY peptide to IL-6 and TNF-α.
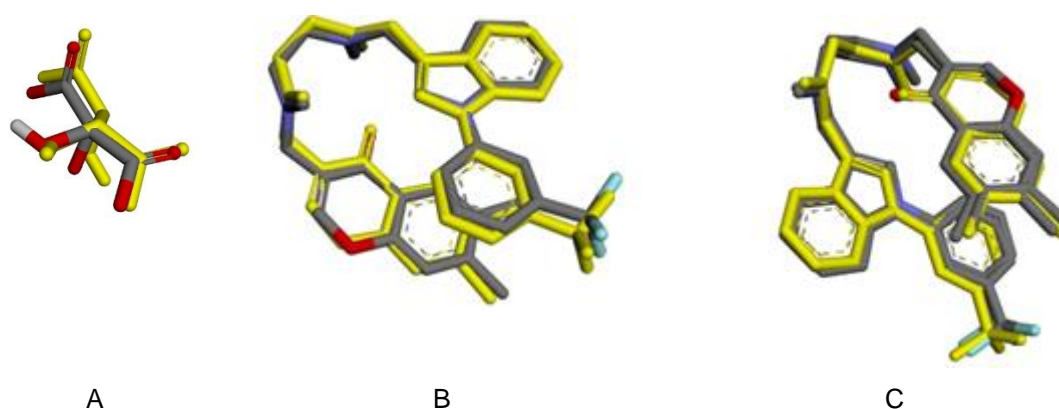

A   B   C

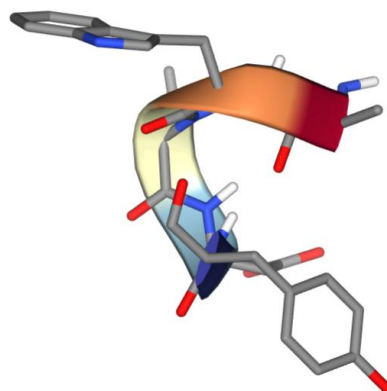**Figure 4.** Comparison of native ligand (A) 1ALU (B) 2AZ5 site 1 (C) 2AZ5 site 2.

Figure 5. PEP-FOLD4 structure of AWVDY.

Docking of the AWVDY compound began with the generation of its 3D peptide structure. The 3D structure of the AWVDY peptide used for the in silico study was obtained through structural optimization using the PEP-FOLD4 application, resulting in an sOPEP energy of –2.28636 (**Figure 5**).

Simulation with PEP-FOLD4 revealed the 3D conformation of a folded peptide [31]. The folding observed in the AWVDY peptide indicated the presence of an alpha-helix structure, arising from interactions between the amino acid residues within the peptide.

The helical folding observed in AWVDY's predicted tertiary structure suggests that the peptide may adopt a more ordered and rigid conformation upon binding to its target receptors. This structural feature could enhance both binding affinity and specificity by improving surface complementarity and enabling the formation of stabilized hydrogen bonding networks. The α-helix motif typically displays side chains in a spatially organized pattern, facilitating directional interactions with receptor residues—particularly relevant when targeting cytokine proteins such as TNF-α and IL-6.

Although molecular docking results indicated the presence of some loop-like flexibility, the intrinsic tendency toward α-helical folding, as shown by the folding simulations, highlights AWVDY's ability to maintain structural balance—rigid enough to ensure stable binding, yet flexible enough to adapt to the dynamic and often shallow binding pockets of cytokines. This dual structural characteristic is likely to contribute to effective engagement with flat and transient protein–protein interaction (PPI) surfaces, which are known to be challenging for conventional small molecules. Hence, the structural profile of AWVDY supports its potential as a peptide-based inhibitor targeting inflammatory signaling pathways.

The molecular docking outcomes are summarized in **Table 2**, which compares the binding affinities of the native ligand, AWVDY peptide, and selected non-steroidal anti-inflammatory drugs (NSAIDs). The receptors used were Interleukin-6 (IL-6, PDB ID: 1ALU) and Tumor Necrosis Factor-alpha (TNF-α, PDB ID: 2AZ5), with the latter evaluated at two distinct binding sites.

The native ligand exhibited the strongest interaction with TNF-α, with binding energies of –13.244 kcal/mol (site 1) and –13.038 kcal/mol (site 2), corresponding to sub-nanomolar inhibition constants (Ki values of 0.201 nM and 0.275 nM, respectively) [39]. These values confirm the high affinity of the native ligand and establish a benchmark for evaluating peptide and drug binding performance. The excellent docking performance of the native ligand further validates the reliability of the docking protocol used in this study.

Table 2. Binding affinity and Inhibiton constant (Ki) to 1ALU and 2AZ5

Compound	1ALU		2AZ5 site 1		2AZ5 site 2	
	Binding affinity (kcal/mol)	Ki	Binding affinity (kcal/mol)	Ki	Binding affinity (kcal/mol)	Ki
Native ligand	-4,529 ± 0,003	481 ± 3.3 µM	-13,244 ± 0,009	0.201 ± 0.002 nM	-13,038 ± 0,011	0.275 ± 0.004 nM
AWVDY	-8,946 ± 0,010	0.270 ± 0.012 µM	-10,372 ± 0,013	23.000 ± 0.3 nM	-10,424 ± 0,005	23.000 ± 0.1 nM
Celecoxib	-7,438 ± 0,017	3.490 ± 0.11 µM	-9,534 ± 0,009	0.099 ±0.001 µM	-9,623 ± 0,011	0.088 ± 0.003 µM
Flurbiprofen	-7,187 ± 0,012	5.360 ± 0.15 µM	-8,244 ± 0,006	0.934 ± 0.009 µM	-8,518 ± 0,020	0.572 ± 0.019 µM
Ibuprofen	-5,592 ± 0,007	78.9000 ± 0.7 µM	-7,452 ± 0,022	3.38 ± 0.16 µM	-7,362 ± 0,006	3.97 ± 0.05 µM

Table 3. Observed virtual screening interaction between ligands and protein.

Compound	Interaction	Observation		
		1ALU	2AZ5 site 1	2AZ5 site 2
Native ligand	Hydrogen Bond	ARG^{A182}, ARG^{A179},GLN^{A175}, ARG^{A40}, CYS^{A44}, ASN^{A48}, CYS^{A50}, ARG^{A30},	GLY^{A121}, TYR^{B59}	GLY^{C121}, GLY^{C122}, GLY^{D121}
	Van der Waals	LEU^{A178}, ASP^{A26}	GLY^{A122}, TYR^{A59}, TYR^{B119}, GLN^{B61}, GLY^{B121}, TYR^{A119}, LEU^{A120}, LEU^{B57}, LEU^{A57}	LEU^{D57}, LEU^{C57}, ILE^{D155}, TYR^{C59}, SER^{C60}, LEU^{C120}, LEU^{D120}, SER^{D60}, TYR^{D119}, GLN^{D61}, TYR^{D151}
AWVDY	Hydrogen Bond	**GLN^{A175}**, LEU^{A33}, ASP^{A34}, **ARG^{A182}**, **ARG^{A30}**, SER^{A37}	TYR^{A151}, SER^{A60}, TYR^{A59}, HIS^{A15}, SER^{B60}, GLN^{A61}, LEU^{B120}, GLN^{A149}	**GLY^{C121}**, TYR^{C151}, GLN^{C61}, TYR^{D119}
	Van der Waals	ASP^{A26}, ARG^{A179}, ASP^{A34}, LEU^{A33}, LYS^{A171}, ARG^{A40}, ILE^{A36}, **LEU^{A178}**	**TYR^{A119}**, GLY^{B121}, LEU^{B57}, **GLY^{A122}**, GLN^{B61}, **LEU^{A120}**, TYR^{B119}, ILE^{A155}	HIS^{C15}, **TYR^{C59}**, **SER^{C60}**, **LEU^{C120}**, GLN^{D61}, **LEU^{D120}**, **TYR^{D151}**, GLY^{C122}, **LEU^{C57}**, **LEU^{D57}**, TYR^{D59}, ILE^{C58}, ILE^{C155}, VAL^{D123}, **ILE^{D155}**, GLY^{D122}, LYS^{D98}
Celecoxib	Hydrogen Bond	ARG^{A30}, SER^{A37}, ARG^{A182}, GLN^{A175}	GLN^{A61}, TYR^{B151}, TYR^{A151}, SER^{A60}, TYR^{A119}, SER^{B60}, TYR^{A59}, ILE^{A155}, LEU^{B57}, GLN^{B61}, TYR^{B119}, GLY^{B121}, LEU^{A120}, LEU^{A57}	TYR^{C151}, GLN^{C61}, TYR^{C119}, GLY^{C121}, GLY^{D121}
	Van der Waals	ASP^{A34}, LYS^{A171}, ASP^{A34}, ASP^{A26}, ILE^{A36}, SER^{A37}, LEU^{A178}, LEU^{A33}, ARG^{A40}, ARG^{A179}		GLN^{D61}, LEU^{D57}, SER^{D60}, TYR^{D119}, LEU^{D120}, LEU^{C120}, SER^{C60}, GLY^{C122}, ILE^{C58}
Flurbiprofen	Hydrogen Bond	ARG^{A179}, ASP^{A34}	LEU^{B120}, TYR^{B151}, GLY^{A121}, TYR^{A151}, GLN^{A61}	LEU^{D120}, GLY^{C121}, TYR^{C151}, GLN^{C61}
	Van der Waals	ASP^{A34}, ARG^{A182}, ARG^{A179}, ARG^{A30}, LEU^{A33}	ILE^{A155}, LEU^{B57}, GLY^{A122}, TYR^{B119}, GLN^{B61}, LEU^{A120}, TYR^{A119}, TYR^{A59}, GLY^{B121}, LEU^{A57}	GLY^{C122}, LEU^{D57}, TYR^{D119}, SER^{D60}, TYR^{D151}, ILE^{C58}, LEU^{C120}, GLN^{D61}, VAL^{D123}, GLY^{D122}, TYR^{D59}, LEU^{C57}, ILE^{C155}
Ibuprofen	Hydrogen Bond	ARG^{A179}, ARG^{A182}, GLN^{A175}	TYR^{B151}, GLY^{A121}, LEU^{B120}	LEU^{D120}, GLY^{C121}
	Van der Waals	LEU^{A178}, GLN^{A175}, ARG^{A182}, ARG^{A30}, SER^{A37}, LYS^{A171}, ASP^{A34}, ARG^{A179}, LEU^{A33}	GLN^{B61}, TYR^{B119}, LEU^{A120}, TYR^{A59}, LEU^{B57}, GLY^{A122}, GLY^{B121}, LEU^{A57}, TYR^{A119}	LEU^{D57}, ILE^{C58}, LEU^{C120}, TYR^{D151}, GLN^{D61}, TYR^{D119}, SER^{D60}, TYR^{D59}, LEU^{C57}, ILE^{C155}, ILE^{D155}, SER^{C60}

Although replicate docking runs were not performed in this study, the binding affinities obtained for AWVDY against TNF-α and IL-6 fall within ranges typically associated with strong molecular interactions. In particular, binding energy values below –9.0 kcal/mol and submicromolar inhibition constants (Ki) for TNF-α are considered indicative of high-affinity binding and potential therapeutic relevance. These findings suggest that AWVDY may inhibit cytokine function at biologically meaningful concentrations, comparable to or exceeding those of some established inhibitors.

Among the NSAIDs evaluated, Celecoxib exhibited the strongest interaction with TNF-α, with Ki values ranging from 0.088 to 0.099 μM, alongside moderate affinity for IL-6 (3.49 μM). This binding profile aligns with Celecoxib's clinical selectivity and supports its mechanistic role in modulating TNF-α–mediated pathways. In contrast, Flurbiprofen and Ibuprofen showed lower binding affinities. Against IL-6, their Ki values were 5.36 μM and 78.9 μM, respectively, and their binding energies for TNF-α were similarly weaker than those of AWVDY and Celecoxib, suggesting limited potential as direct cytokine inhibitors.

The AWVDY peptide demonstrated strong and consistent binding to both cytokines, underscoring its potential as a dual-target inhibitor. Against IL-6 (PDB ID: 1ALU), AWVDY exhibited a binding energy of −8.946 kcal/mol, corresponding to a Ki of 0.270 μM—outperforming all tested NSAIDs in terms of binding strength to this cytokine. Its interactions with TNF-α (PDB ID: 2AZ5) were even more notable, with ΔG values of −10.372 and −10.424 kcal/mol at two binding sites, and a corresponding Ki of 23 nM for both. These values suggest that AWVDY binds not only strongly, but also with high specificity to critical binding regions on TNF-α.

The consistent sub-micromolar Ki values achieved by AWVDY across both receptors emphasize its potential as a lead compound for the development of peptide-based anti-inflammatory therapeutics. Its superior binding performance relative to conventional NSAIDs highlights the growing relevance of peptides in targeting protein–protein interaction (PPI) interfaces, which are often considered undruggable by small molecules due to their shallow, dynamic, and flexible nature.

Mechanistic standpoint, peptides differ fundamentally from small-molecule NSAIDs. While NSAIDs typically inhibit enzyme activity by occupying catalytic pockets, peptides such as AWVDY can engage broader surface areas, allowing them to interfere directly with cytokine–receptor interactions. This feature is particularly advantageous in cytokine targeting, where classical active sites are often absent or poorly defined. Thus, AWVDY's peptide nature may provide unique advantages in disrupting cytokine signaling, a pathway central to many inflammatory and autoimmune diseases.

However, despite the favorable docking energetics, it is important to recognize that computational results alone are not sufficient to predict pharmacological efficacy. Peptides often face limitations related to enzymatic degradation, short systemic half-life, poor cellular permeability, and potential immunogenicity. Future studies should therefore address these pharmacokinetic and pharmacodynamic challenges through stability optimization, delivery system design, and in vitro/in vivo validation to fully realize the therapeutic potential of AWVDY.

The docking simulation results were further analyzed using BIOVIA Discovery Studio 2025 to evaluate the detailed interaction profiles between the ligands and their respective protein receptors (**Table 3**). At the IL-6 binding site (PDB ID: 1ALU), the

native ligand, tartaric acid, formed hydrogen bonds with several key residues, including ARGA182, ARGA179, GLNA175, and ARGA40. The AWVDY peptide displayed a similar binding pattern by forming hydrogen bonds with GLNA175, LEUA33, ASPA34, ARGA182, ARGA30, and SERA37, suggesting that AWVDY may mimic the interaction behavior of the native ligand. Celecoxib also interacted with ARGA30, SERA37, ARGA182, and GLNA175, indicating an overlap in binding residues with AWVDY. Meanwhile, Flurbiprofen and Ibuprofen interacted with ARGA179 and ASPA34, confirming the importance of these residues for ligand anchoring. In addition to hydrogen bonding, van der Waals interactions were consistently observed among all ligands, particularly involving ASPA26, ARGA179, LEUA178, and LYSA171, which highlights the hydrophobic nature of the ligand-binding region at this site.

At TNF-α binding site 1 (PDB ID: 2AZ5), the native ligand formed hydrogen bonds primarily with GLYA121 and TYRB59. In contrast, AWVDY established a broader network of interactions involving TYRA151, SERA60, TYRA59, HISA15, and GLNA61, indicating more extensive surface engagement. Celecoxib and Flurbiprofen also formed multiple hydrogen bonds at this site, engaging with GLNA61, TYRB151, TYRA151, and SERA60, suggesting that these residues play a conserved role in ligand recognition. Ibuprofen formed hydrogen bonds with TYRB151, GLYA121, and LEUB120, reinforcing the relevance of these residues. Van der Waals interactions were broadly shared across compounds,

particularly with GLYB121, TYRB119, and LEUA120, reflecting a common spatial and hydrophobic environment at the binding pocket.

At site 2 of TNF-α, AWVDY formed hydrogen bonds with GLYC121, TYRC151, GLNC61, and TYRD119, many of which were also observed in interactions with Celecoxib and Flurbiprofen. These shared binding residues suggest a conserved binding mechanism at this site. Ibuprofen showed fewer hydrogen bonds but still interacted with critical residues such as GLYC121 and GLNC61. Van der Waals contacts were commonly observed for all ligands at this site, including LEUC120, TYRD119, GLND61, and ILEC155, indicating a consistent hydrophobic environment and stable ligand positioning within the pocket.

Based on the interaction profile, site 1 of TNF-α appears to be more favorable for AWVDY binding than site 2. Site 1 offers a broader range of polar and charged residues for hydrogen bonding—such as TYRA151, HISA15, SERA60, and GLNA61—which can support peptide stabilization through electrostatic and polar interactions. AWVDY forms multiple hydrogen bonds at this site, suggesting strong affinity and favorable orientation. In addition, the van der Waals interactions at site 1 involve a more flexible and extended hydrophobic region, including TYRA119, GLYB121, LEUB57, and ILEA155, which is better suited to accommodate the bulkier and more flexible structure of peptides. In contrast, site 2, although capable of forming stable interactions, presents a more compact and hydrophobically dense pocket with limited

hydrogen bonding diversity, which may restrict optimal binding of a larger, polar peptide like AWVDY.

Despite these differences, AWVDY interacted consistently at both TNF-α sites, with predicted binding energies of −10.372 and −10.424 kcal/mol, raising the possibility of dual-site engagement. Binding at multiple sites—whether simultaneously or sequentially—may enhance overall inhibitory potential by stabilizing alternative conformations of TNF-α or more effectively blocking receptor interaction surfaces. This strategy may also reduce the risk of escape mutations or compensatory signaling, which are common challenges in cytokine-targeted therapies.

AWVDY's intrinsic conformational flexibility allows it to adapt its structure to the molecular environment of each binding site. Docking simulations suggest that AWVDY adopts slightly different conformations at the two TNF-α sites, optimizing interactions specific to each interface. This flexibility is particularly advantageous when targeting the shallow and dynamic protein–protein interaction (PPI) surfaces of TNF-α, which differ significantly from the deep, well-defined pockets targeted by conventional small-molecule drugs.

Compared to previously reported peptide inhibitors of TNF-α—many of which show micromolar binding affinities and target only a single interface—AWVDY's sub-micromolar affinity and dual-site binding are noteworthy. These characteristics suggest the potential for greater potency and specificity. Nevertheless, experimental confirmation using biophysical assays such as surface plasmon resonance (SPR) or NMR spectroscopy is necessary to validate these findings and confirm the proposed dual-binding mechanism.

The strong and consistent binding affinity of AWVDY to TNF-α, along with a Ki value of 23 nM at both binding sites, supports its potential as a potent inhibitor of TNF-α–mediated signaling. Given the central role of TNF-α in diseases such as rheumatoid arthritis (RA) and inflammatory bowel disease (IBD)—where it contributes to chronic inflammation, synovial proliferation, and tissue damage—these findings position AWVDY as a promising therapeutic lead for cytokine-driven autoimmune disorders. While AWVDY also showed significant interaction with IL-6 (ΔG = −8.946 kcal/mol, Ki = 0.270 μM), its stronger and more consistent affinity for TNF-α suggests a degree of selectivity, which could be clinically advantageous in conditions where TNF-α blockade is prioritized, such as moderate-to-severe RA, psoriatic arthritis, and Crohn's disease. Moreover, compared to IL-6–targeting therapies like tocilizumab, which require careful immunomodulation to avoid immune suppression, a TNF-α–selective peptide may offer a more targeted and potentially safer anti-inflammatory profile.

TNF-α and IL-6 are key pro-inflammatory cytokines that play central roles in immune response amplification and regulation [40]. TNF-α initiates and sustains inflammatory signaling by stimulating the production of other cytokines, including IL-6, and by activating immune cells such as macrophages and T-cells. IL-6 acts as both a pro- and anti-inflammatory mediator,

contributing to acute-phase responses, B-cell maturation, and T-cell activation [41]. Persistent elevation of these cytokines is strongly associated with the progression of chronic inflammatory and autoimmune diseases, including RA, IBD, and psoriasis [42, 43]. In this context, peptide-based therapeutics are emerging as promising alternatives to traditional small molecules, offering high target specificity, lower systemic toxicity, and the potential for chemical optimization and modification [44].

While these findings are encouraging, they are based exclusively on in silico docking simulations and should therefore be interpreted with caution. Limitations such as static receptor models, simplified solvation environments, and the absence of entropic and dynamic factors can affect the accuracy of binding predictions. Furthermore, docking studies do not account for crucial pharmacokinetic factors such as enzymatic stability, membrane permeability, or systemic bioavailability. To confirm the biological relevance of AWVDY's predicted activity, follow-up in vitro assays are essential. Recommended next steps include ELISA to quantify binding to TNF-α and IL-6, cell-based assays to assess anti-inflammatory effects, and serum stability tests to evaluate resistance to proteolytic degradation. Together, these experimental approaches would provide critical evidence to validate AWVDY's mechanism of action and support its further development as a peptide-based cytokine inhibitor.

A

B

C

D
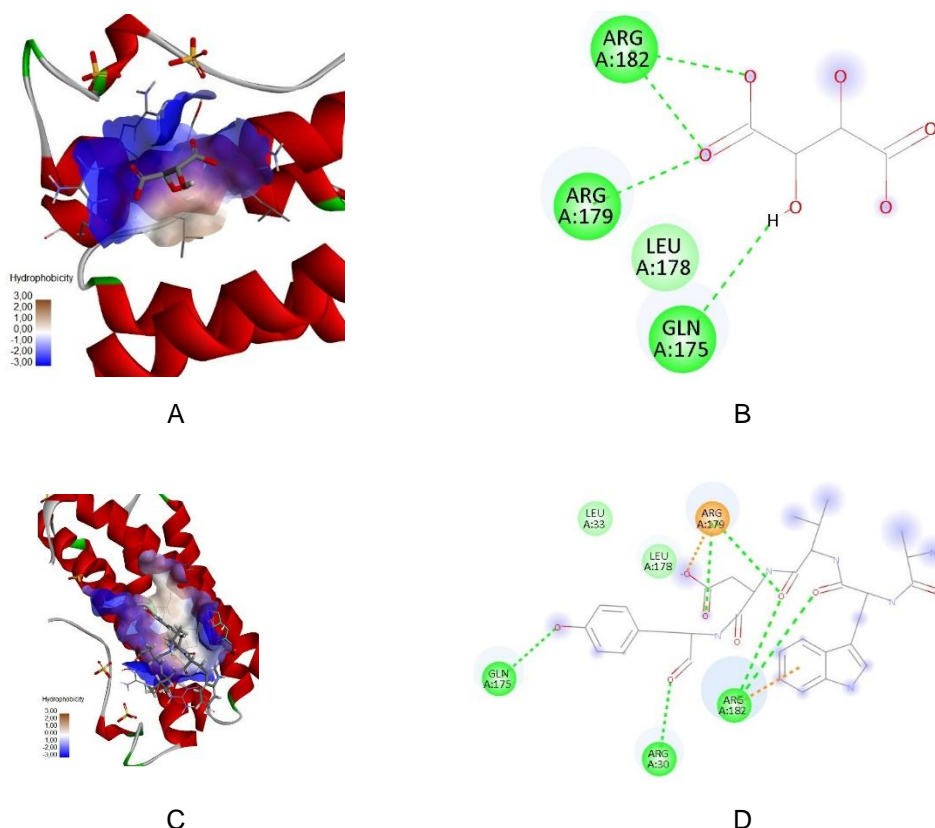
Figure 6. Molecular docking analysis with 1 ALU (A) 3D interaction of native ligand, (B) 2D interaction of native ligand, (C) 3D interaction of AWVDY (D) 2D interaction of AWVDY.
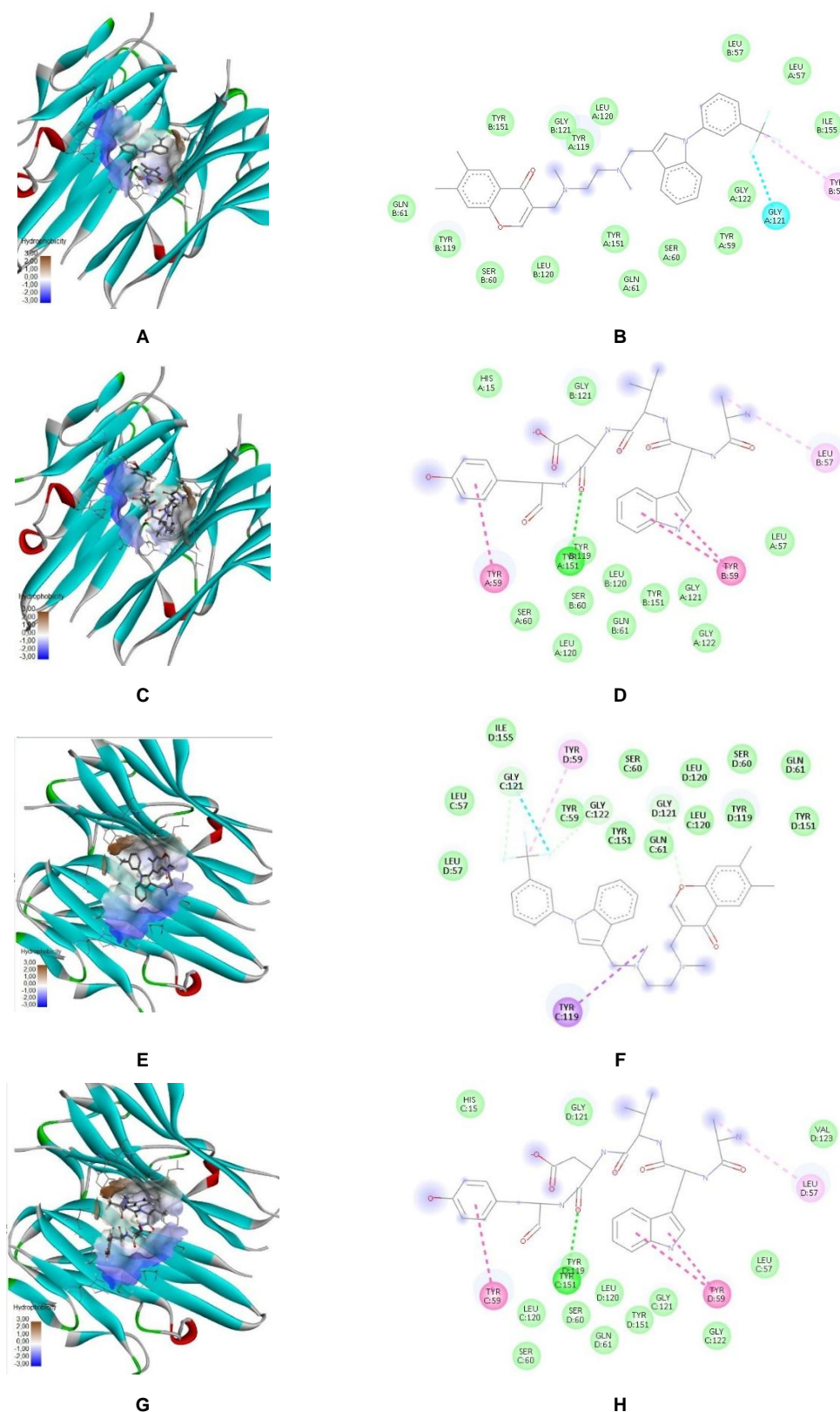
Figure 7. Molecular docking analysis with 2AZ5 (A) 3D interaction of native ligand site 1, (B) 2D interaction of native ligand site 1, (C) 3D interaction of AWVDY site 1, (D) 2D interaction of AWVDY site 1, (E) 3D interaction of native ligand site 2, (F) 2D interaction of native ligand site 2, (G) 3D interaction of AWVDY site 2, (H) 2D interaction of AWVDY site 2.

CONCLUSION

The peptide AWVDY was successfully synthesized using solid-phase peptide synthesis (SPPS) with the Fmoc strategy on 2-chlorotrityl chloride resin, achieving a yield of 95.91% and purity confirmation by HPLC. Molecular docking studies revealed that AWVDY exhibits strong binding affinities of $-10.372 \pm 0,013$, $-10.424 \pm 0,005$, and $-8.946 \pm 0,010$ kcal/mol with TNF-α and interleukin-6 cytokines, suggesting its potential as a lead compound for further investigation as an anti-inflammatory agent, however, further in vitro and in vivo studies are necessary to validate its biological activity and therapeutic efficacy

ACKNOWLEDGE

REFERENCES

[1] S. A. Kviatkovsky et al., "Collagen peptide supplementation for pain and function: is it effective?" *Curr. Opin. Clin. Nutr. Metab. Care*, vol. 25, no. 6, pp. 401–406, Nov. 2022, doi: 10.1097/MCO.0000000000000870.

[2] M. Khatri et al., "The effects of collagen peptide supplementation on body composition, collagen synthesis, and recovery from joint injury and exercise: a systematic review," *Amino Acids*, vol. 53, no. 10, pp. 1493–1506, Oct. 2021, doi: 10.1007/s00726-021-03072-x.

[3] T. Wijesekara et al., "Effect of Bioactive Peptides on Gut Microbiota and Their Relations to Human Health," *Foods*, vol. 13, no. 12, Art. no. 12, Jan. 2024, doi: 10.3390/foods13121853.

[4] P. Luasiri et al., "Exploration of nutritional and bioactive peptide properties in goat meat from various primal cuts during in vitro gastrointestinal digestion and absorption," *Anim. Biosci.*, vol. 37, no. 6, pp. 1096–1109, Jun. 2024, doi: 10.5713/ab.23.0352.

[5] D. Zhu et al., "The dual-function of bioactive peptides derived from oyster (*Crassostrea gigas*) proteins hydrolysates," *Food Sci. Hum. Wellness*, vol. 12, no. 5, pp. 1609–1617, Sep. 2023, doi: 10.1016/j.fshw.2023.02.006.

[6] H. Chen et al., "Protective Effect of Oyster Peptides Derived from Crassostrea gigas on Intestinal Oxidative Damage Induced by Cyclophosphamide in Mice Mediated Through Nrf2-Keap1 Signaling Pathway," *Front. Nutr.*, vol. 9, p. 888960, 2022, doi: 10.3389/fnut.2022.888960.

[7] D. Chatterjee and K. Sivashanmugam, "Immunomodulatory peptides: new therapeutic horizons for emerging and re-emerging infectious diseases," *Front. Microbiol.*, vol. 15, p. 1505571, Dec. 2024, doi: 10.3389/fmicb.2024.1505571.

[8] M. Pavlicevic et al., "Immunomodulatory peptides-A promising source for novel functional food production and drug discovery," *Peptides*, vol. 148, p. 170696, Feb. 2022, doi: 10.1016/j.peptides.2021.170696.

[9] A. L. Wiggenhorn et al., "A class of secreted mammalian peptides with potential to expand cell-cell communication," *Nat. Commun.*, vol.

14, no. 1, p. 8125, Dec. 2023, doi: 10.1038/s41467-023-43857-0.

[10] I. S. Pratama et al., "Bioactive peptides-derived from marine by-products: development, health benefits and potential application in biomedicine," *Fish. Aquat. Sci.*, vol. 25, no. 7, pp. 357–379, 2022, doi: 10.47853/FAS.2022.e33.

[11] H. Huang et al., "Isolation and characterization of antioxidant peptides from oyster (Crassostrea rivularis) protein enzymatic hydrolysates," *Food Sci. Nutr.*, vol. 11, no. 1, pp. 261–273, 2023, doi: 10.1002/fsn3.3058.

[12] L. Yuan et al., "Anti-inflammatory and Antioxidant Activity of Peptides from Ethanol-Soluble Hydrolysates of Sturgeon (Acipenser schrenckii) Cartilage," *Front. Nutr.*, vol. 8, p. 689648, Jun. 2021, doi: 10.3389/fnut.2021.689648.

[13] L. Zheng et al., "Structure–activity relationship of antioxidant dipeptides: Dominant role of Tyr, Trp, Cys and Met residues," *J. Funct. Foods*, vol. 21, pp. 485–496, Mar. 2016, doi: 10.1016/j.jff.2015.12.003.

[14] T. Saisavoey et al., "Antioxidant and Anti-Inflammatory Effects of Defatted Rice Bran (Oryza Sativa L.) Protein Hydrolysates on Raw 264.7 Macrophage Cells," *J. Food Biochem.*, vol. 40, no. 6, pp. 731–740, 2016, doi: 10.1111/jfbc.12266.

[15] A. A. Aloanis et al., "Total Synthesis of Cyclosenegalin A," *ChemistryOpen*, Aug. 2024, doi: 10.1002/open.202400175.

[16] A. A. Aloanis et al., "Alanine-Rich Cyclopeptides: Natural Resources, Bioactivity, Total Synthesis, and Spectroscopy Identification," *ChemistrySelect*, vol. 10, no. 1, p.

e202404379, 2025, doi: 10.1002/slct.202404379.

[17] B. G. de la Torre et al., "Looking Inside the SPPS Reactor through a Refractometer: Online Quantification of the Resin Loading," *Org. Process Res. Dev.*, vol. 29, no. 2, pp. 411–417, Feb. 2025, doi: 10.1021/acs.oprd.4c00431.

[18] Z. Deng et al., "Antihypertensive Effects of Two Novel Angiotensin I-Converting Enzyme (ACE) Inhibitory Peptides from Gracilariopsis lemaneiformis (Rhodophyta) in Spontaneously Hypertensive Rats (SHRs)," *Mar. Drugs*, vol. 16, no. 9, p. 299, Aug. 2018, doi: 10.3390/md16090299.

[19] L. S. Tsutsumi et al., "Solid-phase synthesis of cyclic hexapeptides wollamides A, B and desotamide B," *Tetrahedron Lett.*, vol. 58, no. 27, pp. 2675–2680, Jul. 2017, doi: 10.1016/j.tetlet.2017.05.084.

[20] A. A. Aloanis and V. I. Paat, "Sintesis Siklopeptida," Klaten: Tahta Media, 2024.

[21] N. Mthethwa et al., "Toward sustainable solid-phase peptide synthesis strategy – in situ Fmoc removal," *Green Chem. Lett. Rev.*, vol. 17, no. 1, p. 2325993, Dec. 2024, doi: 10.1080/17518253.2024.2325993.

[22] F. Shahidi and A. Saeid, "Bioactivity of Marine-Derived Peptides and Proteins: A Review," *Mar. Drugs*, vol. 23, no. 4, Art. no. 4, Apr. 2025, doi: 10.3390/md23040157.

[23] C. A. Biji et al, "Anti-inflammatory peptide therapeutics and the role of sulphur containing amino acids (cysteine and methionine) in inflammation suppression: A review," *Inflamm. Res.*, vol. 73, no. 7, pp. 1203–1221, Jul. 2024, doi: 10.1007/s00011-024-01893-6.

[24] I. P. Siwi et al., "Synthesis, molecular docking, and in vitro tests of the Mannich base derivatives of Benzimidazolvanilin as an anti-inflammatory," *J. Penelitian Pendidikan IPA*, vol. 10, no. 4, Art. no. 4, Apr. 2024, doi: 10.29303/jppipa.v10i4.6199.

[25] K. Zia et al., "Identification of potential TNF-α inhibitors: from in silico to in vitro studies," *Sci. Rep.*, vol. 10, no. 1, p. 20974, Dec. 2020, doi: 10.1038/s41598-020-77750-3.

[26] D. Sahu et al., "Novel peptide inhibitor of human tumor necrosis factor-α has antiarthritic activity," *Sci. Rep.*, vol. 14, no. 1, p. 12935, Jun. 2024, doi: 10.1038/s41598-024-63790-6.

[27] M. M. He et al., "Small-Molecule Inhibition of TNF-α," *Science*, vol. 310, no. 5750, pp. 1022–1025, Nov. 2005, doi: 10.1126/science.1116304.

[28] W. Somers et al., "1.9 Å crystal structure of interleukin 6: implications for a novel mode of receptor dimerization and signaling," *The EMBO J.*, vol. 16, no. 5, pp. 989–997, Mar. 1997, doi: 10.1093/emboj/16.5.989.

[29] S.-J. Jiang et al., "A potential peptide derived from cytokine receptors can bind proinflammatory cytokines as a therapeutic strategy for anti-inflammation," *Sci. Rep.*, vol. 9, p. 2317, Feb. 2019, doi: 10.1038/s41598-018-36492-z.

[30] J. Wu et al., "Molecular docking studies of kirenol a traditional Chinese medicinal compound against rheumatoid arthritis cytokine drug targets (TNF-α, IL-1 and IL-6)," *Biomed. Res.*, vol. 28, no. 5, 2017,

[31] J. Rey et al., "PEP-FOLD4: a pH-dependent force field for peptide structure prediction in aqueous solution," *Nucleic Acids Res.*, vol. 51, no.

W1, pp. W432–W437, Jul. 2023, doi: 10.1093/nar/gkad376.

[32] J. Eberhardt et al., "AutoDock Vina 1.2.0: New Docking Methods, Expanded Force Field, and Python Bindings," *J. Chem. Inf. Model.*, vol. 61, no. 8, pp. 3891–3898, Aug. 2021, doi: 10.1021/acs.jcim.1c00203.

[33] R. Agarwal and J. C. Smith, "Speed vs Accuracy: Effect on Ligand Pose Accuracy of Varying Box Size and Exhaustiveness in AutoDock Vina," *Mol. Inf.*, vol. 42, no. 2, p. 2200188, 2023, doi: 10.1002/minf.202200188.

[34] T. Román et al., "Improving 2-Chlorotrityl Chloride (2-CTC) Resin Activation," *Methods Protoc.*, vol. 6, no. 5, p. 82, Sep. 2023, doi: 10.3390/mps6050082.

[35] M. Amblard et al., "Methods and Protocols of Modern Solid-Phase Peptide Synthesis," *Mol. Biotechnol.*, vol. 33, pp. 239–54, Aug. 2006, doi: 10.1385/MB:33:3:239.

[36] D. Carbajo et al., "Optimized Stepwise Synthesis of the API Liraglutide Using BAL Resin and Pseudoprolines," *ACS Omega*, vol. 4, no. 5, pp. 8674–8680, May 2019, doi: 10.1021/acsomega.9b00974.

[37] L. Ferrazzano et al., "Sustainability in peptide chemistry: current synthesis and purification technologies and future challenges," *Green Chem.*, vol. 24, no 5, Feb. 2022, doi: 10.1039/D1GC04387K.

[38] E. M. Terefe and A. Ghosh, "Molecular Docking, Validation, Dynamics Simulations, and Pharmacokinetic Prediction of Phytochemicals Isolated from Croton dichogamus Against the HIV-1 Reverse Transcriptase," *Bioinform. Biol. Insights*, vol. 16, Sep. 2022, doi: 10.1177/11779322221125605.

[39] V. Kairys et al., "Binding affinity in drug design: experimental and computational techniques," *Expert Opin. Drug Discovery*, vol. 14, no. 8, pp. 755–768, Aug. 2019, doi: 10.1080/17460441.2019.1623202.

[40] T. Hirano, "IL-6 in inflammation, autoimmunity and cancer," *Int. Immunol.*, vol. 33, no. 3, pp. 127–148, Dec. 2020, doi: 10.1093/intimm/dxaa078.

[41] E. G. Favalli, "Understanding the Role of Interleukin-6 (IL-6) in the Joint and Beyond: A Comprehensive Review of IL-6 Inhibition for the Management of Rheumatoid Arthritis," *Rheumatol. Ther.*, vol. 7, no. 3, pp. 473–516, Sep. 2020, doi: 10.1007/s40744-020-00219-2.

[42] A. Campanati et al., "Psoriasis as an Immune-Mediated and Inflammatory Systemic Disease: From Pathophysiology to Novel Therapeutic Approaches," *Biomedicines*, vol. 9, no. 11, p. 1511, Oct. 2021, doi: 10.3390/biomedicines9111511.

[43] M. Jarlborg and C. Gabay, "Systemic effects of IL-6 blockade in rheumatoid arthritis beyond the joints," *Cytokine*, vol. 149, p. 155742, Jan. 2022, doi: 10.1016/j.cyto.2021.155742.

[44] A. L. Afonso et al., "The Potential of Peptide-Based Inhibitors in Disrupting Protein–Protein Interactions for Targeted Cancer Therapy," *Int. J. Mol. Sci.*, vol. 26, no. 7, p. 3117, Mar. 2025, doi: 10.3390/ijms26073117.